Draft version July 25, 2018
Typeset using LaTeX **twocolumn** style in AASTeX62

Study of galactic parameter relations in disk-galaxies with different dark matter models

A. Krut,[1,2,3] C. R. Argüelles,[4,2] J. A. Rueda,[1,2,5] and R. Ruffini[1,2,5]

[1] *Dip. di Fisica, Sapienza Università di Roma, Piazzale Aldo Moro 5, I-00185 Rome, Italy*
[2] *ICRANet, Piazza della Repubblica 10, I-65122 Pescara, Italy*
[3] *University of Nice-Sophia Antipolis, 28 Av. de Valrose, 06103 Nice Cedex 2, France*
[4] *Grupo de Astrofísica, Relatividad y Cosmología, Facultad de Ciencias Astronómicas y Geofísicas, UNLP and CONICET Paseo del Bosque S/N 1900, La Plata, Buenos Aires, Argentina*
[5] *ICRANet-Rio, Centro Brasileiro de Pesquisas Físicas, Rua Dr. Xavier Sigaud 150, 22290–180 Rio de Janeiro, Brazil*

(Received July 24, 2018; Revised July 24, 2018; Accepted July 25, 2018)

Submitted to ApJ

Abstract

The study of dark matter (DM) and the way it affects the rotation curve of disk galaxies has unveiled different intricate relations between the dark and baryonic components on galactic scales. Recently, the radial acceleration correlation, found in the SPARC data set by McGaugh et al. (2016), has regained great attention. We show that this correlation and its characteristic scatter can be explained with dark matter composed of self-gravitating fermions in spherical symmetry including the effect of escaping particles. The understanding of the correlation is backed by a goodness of model analysis for 124 filtered galaxies of the SPARC data set, covering different Hubble types. Besides the fermionic DM model, the same kind of analysis is done also for NFW and DC14 models in order to properly compare among them. A better understanding of the nature of the scatter is then given by the analysis of individual galaxies. Following the fermionic DM model (RAR model), we predict several relations for different pairs of structural galaxy parameters including a massive compact core in every galactic center. Of special interest are the $M_{\rm BH}$-$M_{\rm tot}$ relation and the constant surface density law. Recently, Argüelles et al. (2018) showed that the RAR model with a dark matter particle mass of $\sim$50 keV is able to explain them. Here, we are going to enhance these relations with predictions inferred from disk-galaxies of the SPARC data, being below the observable window of the $M_{\rm BH}$-$M_{\rm tot}$ relation.

Keywords: galaxies: halo — galaxies: structure — dark matter

1. INTRODUCTION

The intricate relation between the mass distribution of dark and baryonic (stars, gas) matter on galactic scales, from center to periphery, is an intriguing open question which has gained much attention in the last decade thanks to the vast datasets covering broader radial extents and including for different galaxy types (de Blok et al. 2008; Lelli et al. 2016; Cappellari et al. 2011). Big efforts have been aiming to understand those dark-to-baryonic relations within completely independent approaches. Accordingly, universal relations involving different pairs of structural galaxy parameters have been unveiled for galactic structures.

Focusing on dark components only, Ferrarese (2002) found a link between the total DM mass of a galaxy and the mass of its (massive) dark compact object in the galactic center. This relation covers many order of magnitudes in total DM mass, from $\sim 10^{11}$ (spirals) to $\sim 10^{14}$ (big ellipticals). Additionally, DM halos show a nearly constant surface density $\rho_0 r_h \approx 140^{+80}_{-30}\,{\rm M}_\odot{\rm pc}^{-2}$, where ρ_0 is the central density of the halo core and r_h the one-halo-length-scale of the Burkert profile. This universal halo surface density law is valid over a range of 14 mag in luminosity and for all Hubble types (Donato et al. 2009).

Interestingly, those dark component relations seem to be independent of the obviously existing baryonic mat-

Corresponding author: A. Krut
andreas.krut@icranet.org

ter. But dark and baryonic matter affect their dynamics gravitationally, clearly, what implies possible further relations. Indeed, since the discovery of the $M-\sigma$ relation (Ferrarese & Merritt 2000), supermassive compact objects (e.g. BHs) were considering as main components in galaxy formation and evolution.

Focusing on the outer part of a galaxy, Tully & Fisher (1977) demonstrated an empirical relationship between the stellar mass (or luminosity) and the maximal rotation velocity. Later, it was shown that this Tully-Fisher relation holds even tighter when the gas component is added. Known as baryonic Tully-Fisher relation, it connects the total baryonic mass (stellar and gas) with the maximal rotation velocity (McGaugh et al. 2000). Important to emphasize is that the maximal rotation velocity appears typically as a flat tail in the DM dominated regime. Historically, that flat rotation curve is the classical argument for dark matter because baryonic matter inferred from light implies a Keplerian behavior what is in conflict with observations (Rubin et al. 1980). Thus, it is possible to connect the (baryonic) Tully-Fisher relation with dark matter.

With this idea some authors focus on the mass discrepancy encoded in the magnitude $D = V_{\rm obs}^2/V_{\rm bar}^2$, where $V_{\rm obs}$ is the total observed velocity and $V_{\rm bar}$ is the inferred velocity of the baryonic component only (McGaugh 2004, 2014). They found that for disk galaxies the mass discrepancy shows clearly a systematic increasing ($D > 1$) with decreasing centripetal acceleration of the baryonic component, $a_{\rm bar} = V_{\rm bar}^2/r$, below a particular scale $\mathfrak{a}_0 \approx 1.2 \times 10^{-10}\,{\rm m/s^2}$. Above $\mathfrak{a}_0$ dark matter becomes negligible with $D \approx 1$ where the Keplerian law is recovered. This correlation is known as the mass discrepancy acceleration relation (MDAR).

An alternative representation is the so-called radial acceleration correlation (RAC) what connects the centripetal accelerations of the baryonic and total component. It turned out that this relation, equivalent to MDAR, is independent of the Hubble type. Thus, the relation is not limited to disk galaxies and holds also for other galaxy types (e.g. ellipticals, lenticulars, dwarfs spheroidals) what makes it a true universal law among morphology classification (Lelli et al. 2017b). Despite a relatively large scatter, this relation - independent of the representation - implies a fundamental link between dark and baryonic matter on halo scales what corresponds to the low acceleration regime.

The link arises naturally in Modified Newtonian Dynamics (MOND) and other modified gravity theories (Kroupa 2015; McGaugh et al. 2016; Lelli et al. 2017a) but may be explained within the ΛCDM context as well (Di Cintio & Lelli 2016; Navarro et al. 2016; Salucci 2016). Also hydrodynamical simulations are able to reproduce the radial acceleration correlation (Santos-Santos et al. 2016; Keller & Wadsley 2016; Ludlow et al. 2016; Tenneti et al. 2017).

We face the above problem from a different and complementary perspective relying on semi-analytic approaches which are based on self-gravitating systems of elementary fermions (Argüelles et al. 2018; Ruffini et al. 2015; Siutsou et al. 2015; Argüelles et al. 2014a; Argüelles & Ruffini 2014; Argüelles et al. 2014b). That recently proposed new model (hereafter RAR model) produces novel dark matter distributions with a compact and degenerate core in the galactic center embedded in a finite halo. In other words: a *dense quantum core - classical halo* distribution (or simply *core-halo* distribution hereafter). For a given particle mass range of few $10 - 100\,{\rm keV}$ these continuous core-halo profiles describe halo observables and explain simultaneously the compact core, existing in dwarfs to ellipticals, as an alternative to supermassive black holes (Ruffini et al. 2015; Argüelles et al. 2018). Thus, the RAR model can naturally explain the universal relations involving dark components only, emphasizing the importance of this kind of first principles approaches including quantum statistics, self-gravity and thermodynamics.

It is the purpose of this paper to extend the applicability of the RAR model to universal relations which include both dark and baryonic structural galaxy parameters. We center our attention here in the radial acceleration correlation (McGaugh et al. 2016), broadening the extent of applicability of the RAR from those including only DM as analyzed before. We thus consider a filtered SPARC sample of 2369 data points and apply a non-linear least square statistical analysis in order to check the goodness of fit for the RAR model, making also the same kind of analysis for NFW and DC14 models in order to properly compare among them. The task is then not only to compare between the different approaches but to see what more information can be gained by inspecting the behavior in the (free) physical parameter space of the RAR model depending on some galaxy characteristics.

It is important to emphasize that we focus here on the relation between the acceleration of the dark and baryonic components (instead of the total and baryonic as usually). In this picture characteristic deviations from the empirical radial acceleration correlation are often present in the high acceleration regime (e.g. $V_{\rm obs} \approx V_{\rm bar}$), when inspecting single galaxies. Note that those deviations are qualitatively in contrast to the best-fit of McGaugh et al. (2016) because their analysis is based on data limited by observational methods

what remains the acceleration of the dark matter component poorly resolved in the baryonic matter dominated regime. An additional analysis of the much better resolved Milky Way contributes in a better understanding of the acceleration relation and its characteristic deviations from the best-fit.

Moreover, according to our RAR model we predict a different behavior, compared to the best-fit, in the very low acceleration end and even an increase of the dark matter acceleration in the high acceleration end after the baryonic matter dominated region. The increase is due to the massive quantum core in the galactic center, a fundamental feature of the RAR model. Exactly these deviations are a satisfying explanation of the scatter in the empirical radial acceleration correlation based on the average of many spiral galaxies.

In section 2 (Methodology) we describe the SPARC database, data selection, the halo models we use to fit the inferred DM rotation curve of each galaxy given in the SPARC sample and the fitting methods. The four parametric RAR model is applied for a fixed particle mass ($mc^2 = 50\,\mathrm{keV}$) what reduces the number of free parameters by one. For comparison we consider the NFW model, a two parametric empirical model motivated from N-body simulations (Navarro et al. 1996), and the DC14 model, a baryonic feedback motivated halo model with three free parameters (Cintio et al. 2014).

In section 3 (Results) we present the results of the SPARC analysis, perform a goodness of model analysis to compare the competing dark matter models and give a satisfying explanation for the characteristic deviations (a scatter shower) in the acceleration correlation based on the prototype NGC0055 and the better resolved Milky Way. We also predict relations for different pairs of structural galaxy parameters for the 50keV-RAR model. Of special interest are the M_{BH}-M_{tot} relation (Ferrarese 2002; Kormendy & Bender 2011; Bogdán & Goulding 2015) and the constant surface density relation (Donato et al. 2009). Recently, Argüelles et al. (2018) showed that RAR model is able to explain them for typical galaxies, ranging from dwarfs to elliptical. Here, we are going to enhance these relations with predictions inferred from disk galaxies of the SPARC data set.

Finally, in section 4 (Summary and conclusion) we give a brief summary and conclusion of our results.

2. METHODOLOGY

This work uses the new Spitzer Photometry and Accurate Rotation Curves (SPARC) database. It includes 3.6μm near-infrared and 21 cm observations. The former traces the stellar distribution (bulge and disk) while the latter traces the atomic gas distribution and provides velocity fields from which the rotation curves are derived. See Lelli et al. (2016) for a complete description of the SPARC database.

2.1. *Data selection*

The SPARC data is distributed in separated files and can be found at http://astroweb.cwru.edu/SPARC/. Specific information about each galaxy (i.e Hubble type, inclination etc) are provided in the file Table1.mrt. The information we are interested in, like galactocentric radius r and rotation curves V, are provided in the file Table2.mrt.

In detail, we extract the observed circular velocity V_{obs} and the baryonic contribution V_{bar}, composed of a bulge (V_{b}), disk (V_{d}) and gas component (V_{g}). The bulge and disk components are inferred from surface brightness observations for a given mass-to-light ratio. In sum, the baryonic component is given by

$$V_{\mathrm{bar}}^2 = \Upsilon_{\mathrm{b}} V_{\mathrm{b}}^2 + \Upsilon_{\mathrm{d}} V_{\mathrm{d}}^2 + V_{\mathrm{g}}^2 \tag{1}$$

For convenience, the velocities V_{b} and V_{d} are provided for a mass-to-light ratio of $1\,M_\odot/L_\odot$ what does not represent the real value for a galaxy. Since the mass-to-light ratio is just a constant scaling factor we may correct the velocities simply with the mass-to-light *ratio factors* Υ_b and Υ_d for bulge and disk (in units of $M_\odot/L_\odot$). Then the rotation curve for each component traces immediately its centripetal acceleration $a = V^2/r$.

For the data selection we proceed similar as was done by McGaugh et al. (2016). Thus, we want to note that we consider same mass-to-light ratios since the following data selection output depends on the values. For all bulges we choose $\Upsilon_{\mathrm{b}} = 0.7$ and for all disks $\Upsilon_{\mathrm{g}} = 0.5$ as convenient average representatives. Further, we exclude all galaxies with a bad quality flag ($Q = 3$) and face-on galaxies with an inclination $i < 30°$. Then we exclude all points with a velocity error greater than 10% and all points where the baryonic velocity is greater than 95% of the observed velocity. The latter affects mainly data points in the inner region which is dominated by baryonic matter and strongly depend on the chosen mass-to-light factors. Afterwards, we exclude all remaining galaxies with less then 6 data points and obtain 124 galaxies (out of 174) with 2396 points (of 3355) in total.

2.2. *Halo models*

Following the standard assumption in the literature that baryonic and dark matter do not interact each

other, we calculate the total velocity simply through

$$V_{\rm tot}^2 = V_{\rm bar}^2 + v_{\rm DM}^2 \tag{2}$$

Here, $v_{\rm DM}$ is a theoretical dark matter component.

Three competing dark matter models will be explained in next and compared in the following section.

RAR

Following Ingrosso et al. (1992); Ruffini et al. (2015), a self-gravitating system composed of massive fermions in spherical symmetry is considered. We solve the Einstein equation for a thermal and semi-degenerate fermionic gas considered as a perfect fluid in hydrostatic equilibrium. No additional interaction is assumed for the fermions besides their fulfilling of quantum statistics and the relativistic gravitational equation. The static metric given in the standard form is

$$g_{\mu\nu} = {\rm diag}(e^{\nu(r)}, -e^{\lambda(r)}, -r^2, -r^2\sin^2\vartheta) \tag{3}$$

where $\nu(r)$ and $\lambda(r)$ depend only on the radial coordinate r. For this metric the circular velocity is simply given by

$$\frac{v^2(r)}{c^2} = \frac{1}{2}\frac{{\rm d}\nu}{{\rm d}\ln[r/R]} \tag{4}$$

In next, we assume that the stress tensor is described by a perfect fluid in equilibrium. According to this TOV (Tolman-Oppenheimer-Volkoff) approach the metric potential $\nu(r)$ is described by the important relation

$$\frac{{\rm d}\nu}{{\rm d}r/R} = \frac{R^2}{r^2}\left[\frac{M(r)}{M} + \frac{r^3}{R^3}\frac{P(r)}{\rho c^2}\right]\left[1 - \frac{R}{r}\frac{M(r)}{M}\right]^{-1} \tag{5}$$

The enveloped mass within a given radius r, which we call hereafter simply the mass $M(r)$, is given by

$$\frac{\rm d}{{\rm d}r/R}\frac{M(r)}{M} = \frac{r^2}{R^2}\frac{\rho(r)}{\rho} \tag{6}$$

Further, mass density and pressure are represented in terms of statistical physics (Shapiro & Teukolsky 2008),

$$\frac{\rho(r)}{\rho} = \frac{4}{\sqrt{\pi}}\int_1^\infty \epsilon^2\sqrt{\epsilon^2-1}f(r,\epsilon){\rm d}\epsilon \tag{7}$$

$$\frac{P(r)}{\rho c^2} = \frac{4}{3\sqrt{\pi}}\int_1^\infty (\epsilon^2-1)^{3/2}f(r,\epsilon){\rm d}\epsilon \tag{8}$$

where $\epsilon^2 = 1 - p^2/mc^2$ describes the particle energy with rest mass (in units of mc^2) and $f(r,\epsilon)$ is a phase space distribution function. Here, we introduced the scaling factors R, M and ρ related by

$$\frac{R}{l_{\rm P}} = g^{-1/2}\pi^{1/4}\frac{m_{\rm P}^2}{m^2} \tag{9}$$

$$\frac{M}{m_{\rm P}} = \frac{1}{2}g^{-1/2}\pi^{1/4}\frac{m_{\rm P}^2}{m^2} \tag{10}$$

$$\frac{\rho}{\rho_{\rm P}} = \frac{1}{8}g\pi^{-3/2}\frac{m^4}{m_{\rm P}^4} \tag{11}$$

with the Planck scales for mass ($m_{\rm P}$), length, ($l_{\rm P}$) and density ($\rho_{\rm P} = m_{\rm P}/l_{\rm P}^3$). For mass and length we may use the equivalent relation $2GM/R = c^2$ where G is the gravitational constant and c is the speed of light. m is the particle mass and g is the particle degeneracy. For fermions we have $g = 2$.

In order to solve the metric potential (5) we consider the Fermi-Dirac distribution with cutoff,

$$f(r,\epsilon) = \left[1 - e^{[\epsilon-\varepsilon(r)]/\beta(r)}\right]\left[e^{[\epsilon-\alpha(r)]/\beta(r)} + 1\right]^{-1} \tag{12}$$

for $\epsilon \le \varepsilon(r)$. Here, $\beta(r) = k_B T(r)/mc^2$ is the temperature parameter, $\alpha(r)$ describes the chemical potential (with rest mass) and $\varepsilon(r)$ we call the cutoff energy (with rest mass). All three parameters are related with the metric potential through the Tolman relation (Tolman & Ehrenfest 1930), the Klein relation (Klein 1949) and the conservation of energy (Merafina & Ruffini 1989). In detail,

$$\frac{{\rm d}\ln\beta(r)}{{\rm d}r/R} = \frac{{\rm d}\ln\alpha(r)}{{\rm d}r/R} = \frac{{\rm d}\ln\varepsilon(r)}{{\rm d}r/R} = -\frac{1}{2}\frac{{\rm d}\nu}{{\rm d}r/R} \tag{13}$$

In next, it is convenient to introduce the degeneracy parameter $\theta(r)$ and the cutoff parameter $W(r)$ defined by

$$\theta(r) = \frac{\mu(r)}{k_B T(r)} \tag{14}$$

$$W(r) = \frac{E_c(r)}{k_B T(r)} \tag{15}$$

where $E_c(r)$ is the classical particle escape energy (King 1966).

Chemical potential and cutoff energy become then $\alpha(r) = 1+\beta(r)\theta(r)$ and $\varepsilon(r) = 1+\beta(r)W(r)$. Here, $\mu(r)$ is the chemical potential (with rest mass subtracted), $T(r)$ is the temperature and k_B is the Boltzmann constant.

Note that a distribution function of the kind of eq. (12) can be obtained as a (quasi) stationary solution of a generalized Fokker-Planck equation for fermions including the physics of violent relaxation and evaporation, appropriate to treat non-linear galactic DM halo structure formation (Chavanis 2004).

Finally, the metric potential is solved numerically with the initial condition

$$M(0) = 0, \quad \beta(0) = \beta_0, \quad \theta(0) = \theta_0, \quad W(0) = W_0 \tag{16}$$

Besides those configuration parameters (β_0, θ_0, W_0) the RAR model is described also by the particle mass m, which is necessary to provide right physical properties for the obtained configurations. However, we set the particle mass to $mc^2 = 50\,\mathrm{keV}$ as a promising candidate motivated by the the recent application of the RAR model to different types of galaxies from dwarfs to ellipticals (**?**).

DC14

The DC14 model is given by a slightly modified Hernquist model which includes the influence of galaxy formation based on more profound baryonic feedback mechanism (Cintio et al. 2014; Katz et al. 2016; Hernquist 1990)

$$\frac{\rho(r)}{\rho_\mathrm{N}} = \left[\frac{r}{R_\mathrm{N}}\right]^{-\gamma} \left[1 + \left[\frac{r}{R_\mathrm{N}}\right]^{\alpha}\right]^{-\frac{\beta-\gamma}{\alpha}} \tag{17}$$

The three parameters (α, β, γ) are related through the stellar-to-dark matter ratio encoded via $X = \log_{10}(M^*/M_\mathrm{halo})$,

$$\alpha = 2.94 - \log_{10}\left[(10^{X+2.33})^{-1.08} + (10^{X+2.33})^{2.29}\right] \tag{18}$$

$$\beta = 4.23 + 1.34X + 0.26X^2 \tag{19}$$

$$\gamma = -0.06 - \log_{10}\left[(10^{X+2.56})^{-0.68} + 10^{X+2.56}\right] \tag{20}$$

The velocity is described by a hyper geometric function,

$$\frac{v^2(r)}{\sigma_\mathrm{N}^2} = \frac{1}{3-\gamma}\left[\frac{r}{R_\mathrm{N}}\right]^{3-\gamma} {}_2F_1(p_1, p_2;\, q_1;\, -[r/R_\mathrm{N}]^\alpha) \tag{21}$$

with

$$\begin{aligned} p_1 &= (3-\gamma)/\alpha \\ p_2 &= (\beta-\gamma)/\alpha \\ q_1 &= 1 + (3-\gamma)/\alpha \end{aligned}$$

NFW

The NFW model is simply given by (Navarro et al. 1996)

$$\frac{\rho(r)}{\rho_\mathrm{N}} = \left[\frac{r}{R_\mathrm{N}}\right]^{-1} \left[1 + \frac{r}{R_\mathrm{N}}\right]^{-2} \tag{22}$$

with the circular velocity

$$\frac{v^2(r)}{\sigma_\mathrm{N}^2} = \frac{\ln(1 + r/R_\mathrm{N})}{r/R_\mathrm{N}} - \frac{1}{1 + r/R_\mathrm{N}} \tag{23}$$

Here, NFW and DC14 use the newtonian scaling factors: R_N, ρ_N, $\sigma_\mathrm{N}^2 = GM_\mathrm{N}/R_\mathrm{N}$ and $M_\mathrm{N} = 4\pi\rho_\mathrm{N}R_\mathrm{N}^3$ are the scaling factors for length, density, velocity and mass.

2.3. *Data fitting*

We fit the inferred DM rotation curve, $V_\mathrm{DM}^2 = V_\mathrm{obs}^2 - V_\mathrm{obs}^2$, with the Levenberg–Marquardt (LM) algorithm to find a χ^2 minima. The quantity χ^2 is calculated by

$$\chi^2(\boldsymbol{p}) = \sum_{i=1}^{N}\left[\frac{V_i - v(r_i, \boldsymbol{p})}{\sigma_i}\right]^2 \tag{24}$$

with N the number of data points, V_i is the set of circular velocity data, r_i is the corresponding set of radius data, $v(r_i, \boldsymbol{p})$ is the predicted circular velocity at radius r_i for the model parameter vector $\boldsymbol{p}$ and σ_i is the uncertainty for V_i.

For the RAR model, $\boldsymbol{p} = (\theta_0, W_0, \beta_0, m)$, we vary the three free parameter (θ_0, W_0, β_0) for a fixed particle mass m. Due to numerical stability improvements we consider the cutoff parameter $W_0 = 1.73\theta_0 + 1.07 + 10^\omega$ to make sure our fitting algorithm obtains only solutions with a halo (for approx. $W_0 < 1.73\theta_0 + 1.07$ the halo gets disrupted and only a degenerate core remains). Phenomenally, we can vary the cutoff through the cutoff parameter W_0 and the steepness through the degeneracy parameter θ_0. The latter is only possible within the transition regime ($\theta_0 \in [-5, 15]$). For high degeneracy, $\theta_0 > 15$, we obtain a cored halo with a degenerate core. For these degenerate solutions we propose a particle mass of $m = 50\mathrm{keV/c}^2$ as a promising candidate (**?**).

The NFW model describes a fixed cuspy halo with two free scaling parameter, e.g. $\boldsymbol{p} = (R_N, \rho_N)$. Therefore, that model can not explain the variation of the inner RC steepness or the variation in the cutoff. Instead, it is expected that NFW covers the rotation curves well on average due to its wide maxima bump.

The DC14 model, e.g. $\boldsymbol{p} = (X, R_N, \rho_N)$, has the additional parameter X compared to NFW which affects the inner steepness and the maxima bump width simultaneously.

For the LM fitting algorithm we need well chosen initial values to ensure convergence. Because that algorithm finds only local minima we choose 100 parameter sets randomly within a range. For the RAR model we have $\theta_0 \in [25, 45]$, $\beta_0 = [10^{-8}, 10^{-5}]$ and $\omega \in [0, 2]$. For NFW we have $R_N \in [10^1, 10^4]$, and $\rho_N = [10^{-4}, 10^{-1}]$. For the DC14 model we choose the same ranges as for the NFW model. Also, according to Katz et al. (2016)

we may bound the initial values of the additional parameter to $X \in [-3.75, -1.3]$. These ranges are no restrictions such that the fitting algorithm may find solutions beyond the boundaries.

3. RESULTS

Here, we reproduce the radial acceleration correlation and perform a goodness of model analysis for our RAR model as well as for NFW and DC14. We demonstrate that the acceleration behavior for individual galaxies is more intricate what becomes obvious after changing the perspective of the acceleration correlation. Finally, we present correlations for different pairs of structural galaxy parameter.

3.1. *Acceleration correlations*

The radial acceleration correlation (hereafter RAC) compares the total acceleration $a_{\rm tot}$, implying all matter contribution, with the baryonic component $a_{\rm bar}$, see top panels of fig. 1. The correlation in this projection ($a_{\rm tot}$-$a_{\rm bar}$) is well described by McGaugh's empirical fit McGaugh et al. (2016),

$$a_{\rm tot} = \frac{a_{\rm bar}}{1 - {\rm e}^{-\sqrt{a_{\rm bar}/\mathfrak{a}_0}}} \tag{25}$$

with the only parameter $\mathfrak{a}_0 \approx 1.20 \times 10^{-10}\,{\rm m/s^2}$. It clearly shows a deviation from the linear correlation, inferred from spiral galaxies, in the low acceleration regime ($a_{\rm bar} \ll \mathfrak{a}_0$), what is dominated by dark matter. In the high acceleration regime ($a_{\rm bar} \gg \mathfrak{a}_0$), where baryonic matter dominates, the linear relation is recovered.

An equivalent representation of the link between baryonic and total components is given by the mass discrepancy acceleration relation (hereafter MDAR). It is usually defined as the ratio between the total velocity and the baryonic velocity, $D = V_{\rm tot}/V_{\rm bar}$. With $a = v^2/r$ this relation is equivalent to $D = a_{\rm tot}/a_{\rm bar}$ and the results are illustrated in the bottom panels of fig. 1. In the limiting case of spherical mass distributions and with $a = \frac{{\rm d}\Phi}{{\rm d}r}$ the relation may be linked to the enclosed masses through $D = M_{\rm tot}/M_{\rm bar}$.

According to our results we conclude that all considered models (RAR,NFW,DC14) are able to reproduce the acceleration correlations (RAC and MDAR). Qualitatively, they look similarly good compared to the empirical correlation (25) inferred from original SPARC data. Especially, the deviation in the low acceleration regime look adequate, representing the dark matter dominated region. Unsurprisingly, the linear relation in the high acceleration regime, representing the baryonic matter dominated region, is reproduced as well. This is obvious because the DM halo models predict mass profiles with negligible DM contribution in the inner disk region towards the bulge.

Indeed, according to some authors RAC and MDAR does not show any new physics and may be explained within the ΛCDM framework (Navarro et al. 2016; Keller & Wadsley 2016; Salucci 2016). Based on modern cosmological simulations, Keller & Wadsley (2016) predict even a redshift dependency of the acceleration parameter $\mathfrak{a}_0$ what emphasizes that the correlation is universal only regarding the morphological classification.

Both, the RAC and MDAR, have been criticized that their representation focus only on the low acceleration regime where dark matter dominates. Therefore, Chae et al. (2017) suggested to compare the baryonic component, $a_{\rm bar}$, with the ratio of the baryonic and dark matter components, $a_{\rm DM}/a_{\rm bar}$, what gives also information about dark matter in the intermediate acceleration regime. They clearly realized that the original representation of RAC/MDAR shows a fundamental link on halo scales but simultaneously obscures the relation between dark and baryonic matter on inner halo scales. Therefore, any DM model independent of the inner shape (cored or cuspy) would reproduce the linear relation in the baryon dominated region.

Following that argument we suggest a similar approach. Thus, we want to emphasize that it is more convenient to connect directly the dark matter component, $a_{\rm DM} = a_{\rm obs} - a_{\rm bar}$, with the baryonic counterpart $a_{\rm bar}$. This reveals more information about the relation between baryonic and dark matter ranging from the low acceleration up to the high acceleration regime. Especially details about the DM acceleration in the baryon dominated part are unveiled. In this presentation we find (on a first glimpse) a linear correlation in the loglog-plot rather than the empirical fit proposed by McGaugh et al. (2016). The important fact remains that a radial acceleration correlation is found and ranges from a DM dominated region to a baryonic matter dominated region, see middle panels of fig. 1. Contrasted with the original representation we noticed an increased scatter (in form of a *scatter shower*) in the high acceleration regime which we are going to analyze in more detail.

Finally, we want to note that regardless of the presentation ($a_{\rm tot}$ or $a_{\rm DM}$) it is difficult to compare the different DM models quantitatively with respect to the acceleration correlation found in the SPARC database due to the increased scatter. Qualitatively they all are able to explain that correlation. In next, the strategy therefore is to focus on the dark matter fit of the rotation curves (rather than the inferred acceleration correlation) and assign for each fit numerical values what allows a quantitative comparison of the dark matter models.

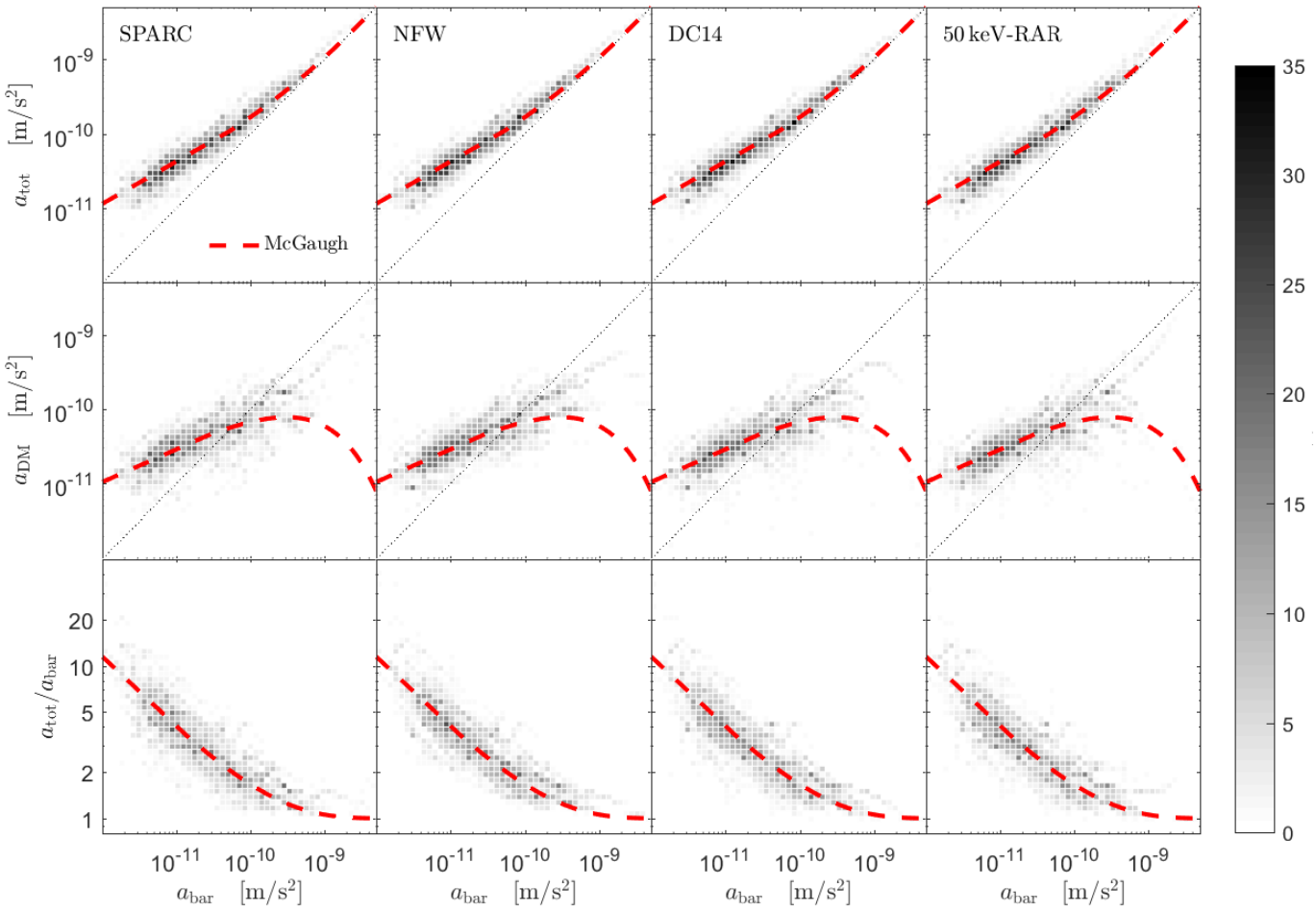

Figure 1. Radial acceleration correlations from SPARC data (first row), NFW (second row), DC14 (third) and RAR (forth row). The correlation is presented in three different ways: (top panels) original correlation with focus on the total acceleration $a_{\rm tot}$, (middle panels) correlation with focus on the dark component $a_{\rm DM}$ and (bottom panels) the mass discrepancy acceleration relation with focus on the ratio $a_{\rm tot}/a_{\rm bar}$. The baryonic centripetal acceleration $a_{\rm bar}$ is inferred from luminosity observables while the total acceleration is inferred from velocity fields. Both measurements are independent. For SPARC data the inferred DM acceleration is given by $a_{\rm DM} = a_{\rm obs} - a_{\rm bar}$. In the case of RAR, NFW and DC14 the total acceleration is composed of the predicted dark and the inferred baryonic components. Each plot is divided in 50x50 equal bins showing clearly a non-linear correlation. Note, that the top panels emphasize mainly the dark matter dominated region for accelerations below the particular value $\mathfrak{a}_0 \approx 1.20\times10^{-10}$m/s^2. Above that acceleration the information about dark matter is hidden due to the baryon dominance, what becomes unveiled in the middle panels. Qualitatively, all considered models (RAR,NFW,DC14) are able to reproduce the radial acceleration correlation, independent of the representations.

3.2. *Goodness of model*

The SPARC galaxies show several phenomena in their rotation curves. Some galaxies indicate a clear cutoff in the outer halo and/or a variation of the inner halo steepness, giving hints of a cored or cuspy halo. Many galaxies show a rising tail implying that the rotation curves are incomplete. This is most probably due to faint stars in the outer most halo region. On the other hand, some galaxies are characterized by a clear oscillation in their flat rotation curve. Of interest is therefore a quantitative description about the goodness of a model fitting the entire galaxy sample.

The goodness of a fit for a single galaxy is well described by the χ^2 value. When competing models with different number of parameters are compared it is appropriate to consider the reduced χ^2 defined as $\chi^2_r = \chi^2/d$ with the degree of freedom $d = N - p$, N the number of observables (for a single galaxy) and p the number of parameters (of the considered model). The question now arises how to compare the competing models for a population of galaxies. Clearly, the sum of (reduced) χ^2 values for a model would be an inappropriate indica-

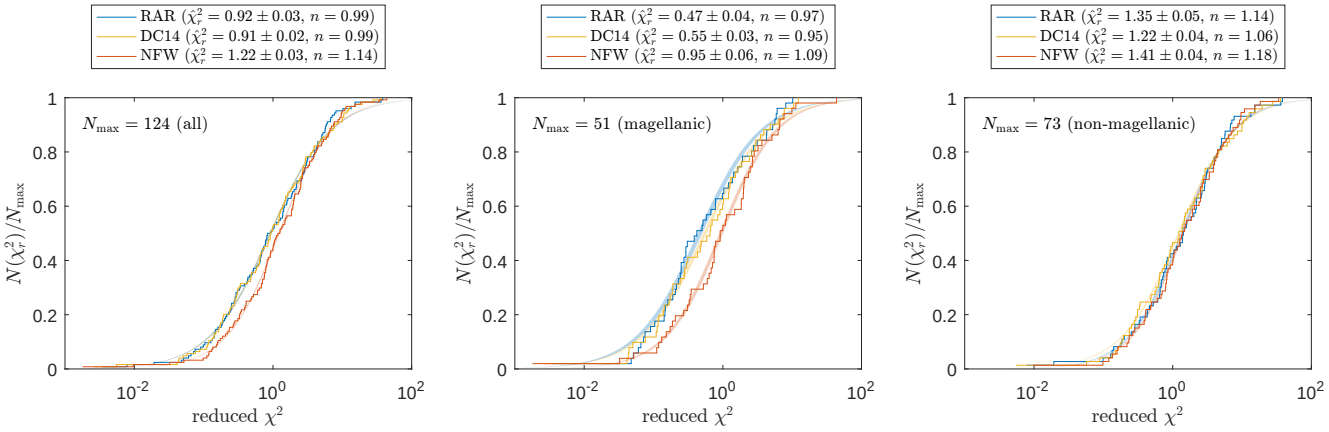

Figure 2. Goodness of model analysis for all galaxy types (left), only magellanic (middle) and non-magellanic (right). We count the population of fitted galaxies having a reduced χ^2 smaller than a given one. The normalized population may be well described by the function $1/[1+(\chi_r^2/\hat{\chi}_r^2)^{-n}]$ with the median $\hat{\chi}_r^2$ and the supplemental descriptor n. RAR and DC14 are similarly good when the galaxy type is ignored. NFW, in contrast, is clearly disfavored here. This picture becomes much more obvious when only magellanic types are considered. On the other hand, focusing on non-magellanic types there is no clear favorite.

tor. Consider the case where a model fits the majority of a population very well (low χ^2 values) but fails extremely (very high χ^2) for just a few galaxies. Thus, the goodness of a model cannot depend on the whole population. Instead, we have to look differentiated at the population. Therefore, we ask *how many* fitted galaxies have a (reduced) χ^2 *lower* than a given one. It turns out that the normalized population curve may be well described by the function

$$\frac{N(\chi_r^2)}{N_{\rm max}} = \frac{1}{1+\left[\frac{\chi_r^2}{\hat{\chi}_r^2}\right]^{-n}} \tag{26}$$

The parameter $\hat{\chi}_r^2$ cuts the population in half where the first half has a lower reduced χ^2 and the other half has a greater reduced χ^2 compared to the median $\hat{\chi}_r^2$. Exactly this criteria is used to described the goodness of a model for fitting a population of galaxies. Thus, we use $\hat{\chi}_r^2$ to compare the competing models (RAR, DC14, NFW). The secondary parameter n is a descriptor for the population distribution itself. It tells, how bad the first half of the population is fitted and how good the other half. The higher n the steeper is the slope of the curve at $\hat{\chi}_r^2$. A high n value would imply that the fits of most galaxies have a reduced χ^2 slightly greater than the median $\hat{\chi}_r^2$. In other words, a high n value imply that the considered model fits all galaxies similarly good with a reduced χ^2 around the median $\hat{\chi}_r^2$. There would be only few very good fits and same for very bad fits compared to $\hat{\chi}_r^2$. Thus, the descriptor n is a supplemental parameter, which gives further information about a model, but it is not useful to compare different models like $\hat{\chi}_r^2$.

The introduced method is similar to the empirical distribution function when the normalized population is interpreted as a probability depending on the variable χ_r^2.

The goodness of the competing models (RAR, DC14, NFW) in fitting the SPARC galaxy sample is summarized in fig. 2. RAR and DC14 are similarly good when the morphological type is ignored. NFW, in contrast, is clearly disfavored here. This picture becomes much more obvious when only megallanic types (Sd,Sdm,Sm,Im) are considered. On the other hand, focusing on non-megallanic types (S0,Sa,Sab,Sb,Sc,Scd,BCD) there is no clear favorite. This implies a connection between dark matter and the morphological type. Moreover, comparing DC14 and NFW implies that baryonic feedback is an important mechanism for galaxy formation. On the other hand, our results show that the RAR model is as good as DC14 although it doesn't consider any baryonic matter contribution nor any baryonic feedback mechanism.

Galaxies of magellanic type which are fitted very well, especially, by the RAR model are NGC0055 (Sm), UGC05986 (Sm), UGC05750 (Sdm), UGC05005 (Im), F565-V2, (Im), UGC06399 (Sm), UGC10310 (Sm), UGC07559 (Im), UGC07690 (Im), UGC05918 (Im) and UGC05414 (Im). This bolsters the results of the goodness of model analysis in fig. 2.

A Remarkably good fit with the RAR model (and DC14) is given for NGC0055 (Sm), see figs. 3 and 4. We now focus on this particular prototype to investigate the large scatter in the radial acceleration correlation. The prototype demonstrates that many galaxies don't follow strictly McGaugh's empirical formula for the acceleration correlation. While in the DM dominated regime ($a_{\rm bar} < \mathfrak{a}_0$) the acceleration relation seems to be close to

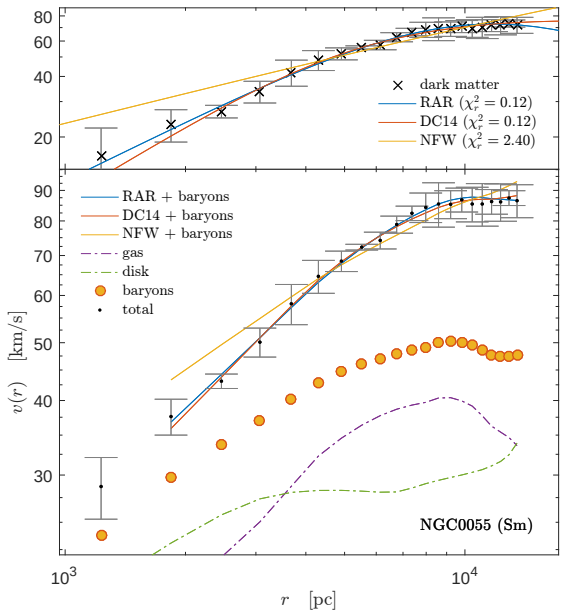

Figure 3. Rotation curve of NGC0055 with total velocity and baryonic components (bottom). The sum of dark and baryonic components give the total velocities (thick solid lines). The best fitted DM components (top) are given for RAR, NFW and DC14, being compared with the inferred DM from SPARC data. RAR and DC14 produce very similar results despite the underlying physics. NFW is is clearly disfavored here, especially in the inner halo.

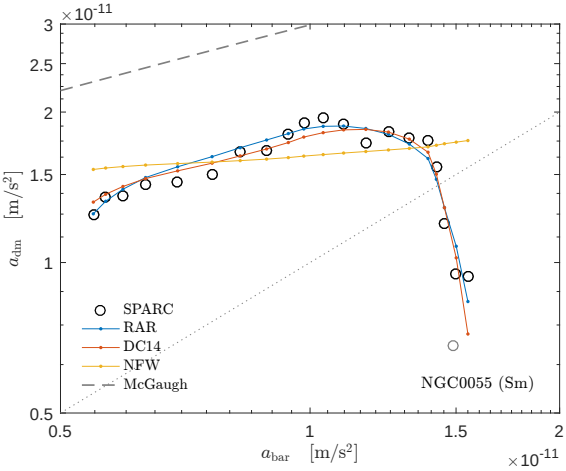

Figure 4. Radial acceleration curve of NGC0055 with SPARC data (circles), McGaugh's empirical fit (dashed line, see eq. (25)) and best fits of the considered DM models. The dotted line shows where dark matter and baryonic accelerations are equal. RAR and DC14 produce very similar results while NFW is disfavored here (compare fig. 3).

McGaugh's fit (despite an offset) we find an abrupt decrease just before the baryon dominated regime. These abrupt decreases we interpret as the source of the increased scatter, especially in form of a *scatter shower* in the low acceleration regime of dark matter. RAR and DC14 can reproduce that abrupt decrease very well, but NFW has serious problems in the baryon dominated regime what is due to its cuspy design. An interesting characteristic of the rotation curve is its slope in the inner halo (baryon dominated region) what shows the nature of the halo: cored or cuspy. The RAR model implies a cored halo and is therefore good in fitting those halos. Contrary, the NFW model gives by design a cuspy halo. For the RAR model (with a well defined halo) as well as for the NFW model those inner halo slopes are fixed while DC14 is more flexible. In sum, the prototype NGC0055 demonstrates clearly that the inner halo shape is important when the relevance of a cuspy or cored halo is considered. It should be now obvious that the new perspective of the radial acceleration correlation ($a_{\rm bar} - a_{\rm DM}$) is preferred compared to the original ($a_{\rm bar} - a_{\rm obs}$) which obscures the inner halo relation.

Another interesting phenomena are oscillations in the rotation curve (RC). Most galaxies, which are poorly fitted by any of the considered models, show *short range* oscillations with more than one maxima in their RC. None of the models can explain that phenomena found mostly in non-magellanic galaxy types: e.g. NGC2403 (Scd), UGC02953 (Sab), NGC6015 (Scd), UGC09133 (Sab), UGC06787 (Sab), UGC11914 (Sab), NGC1003 (Scd), NGC0247 (Sd), UGC08699 (Sab) and UGC03205 (Sab). Indeed, all models show only one maxima in their RC within the range of interest. Phenomenally, in the RAR model it is possible to vary the width of the maxima bump in the RC through the cutoff parameter W_0 in the strong cutoff regime. But without or with weak cutoff the RAR model shows long range oscillations, equivalent to the IS model. However, these oscillations are too long and therefore not a convenient explanation. On the other hand, in the case of strong cutoff we obtain a narrow maxima bump necessary for many RCs, especially for galaxies of magellanic type which do not show those oscillations in general, e.g. NGC0055 (Sm), UGC05986 (Sm), UGC07323 (Sdm), KK98-251 (Im), DDO168 (Im), D631-7 (Im), DDO161 (Im), UGCA442 (Sm), DDO154 (Im), F583-1 (Sm), but also for non-magellanic galaxy types, e.g. NGC5585 (Sd), NGC7793 (Sd), UGC06614 (Sa), ESO079-G014 (Sbc), F571-8 (Sc), NGC0891 (Sb), UGC06614 (Sa), UGC09037 (Scd), NGC4217 (Sb), UGC04278 (Sd). NFW has a wide maxima bump and fits therefore oscillating RC well only on average. Same for DC14 since it may vary the maxima

bump width. Exactly these oscillations — or a lack of them — may be an interesting hint for the connections between dark matter and the morphological type as suggested by the goodness of model analysis, see fig. 2.

3.3. χ^2 *analysis*

We are moving now to a more detailed χ^2 analysis of three selected galaxies, each representing some characteristics of given observational data in relation to the RAR model fit. Thus, we mainly divide the SPARC galaxies in three group through the inferred dark matter component as explained in next.

The first group, represented by NGC0055, clearly shows only a single maxima in its dark matter rotation curve. As shown in fig. 5 this typical profile is well fitted by the RAR model with sufficient low cutoff values, corresponding to not negligible surface effects. However, due to the lack of information in the inner halo structures, especially the galactic center, there is some uncertainty in the strength of the cutoff parameter. Although those solutions provide a minimal DM halo mass, the uncertainty is physically better reflected in the core mass M_c, what covers a range of about two orders of magnitude. Higher core masses, given for lower W_0 values, imply cuspier halos what are clearly discarded here. Well disfavored are also higher DM halo masses M_s which corresponding to isothermal-like halos, given for higher W_0 values. In contrast, those solutions provide a minimal core mass M_c with a huge uncertainty in the total mass.

The second group, represented by DDO161, shows a rising part in the rotation curve towards a maximum without a clear turning point, compared to the first group. Fitting those galaxies for different W_0 values does not necessary favor solution with or without surface effects. The variation in the χ^2 value remains rather small, see fig. 6. Nevertheless, clearly discarded are cuspy halos just as in the first group. There is a narrow χ^2 minimum for relatively low W_0 values suggesting a best-fit. However, this result should be taken with caution because the obtained minimum depends on the inner data points, keeping in mind that for most galaxies in the SPARC data base the inner data points have a relatively high uncertainty. This is also the case for DDO161.

Finally, the third group, represented by NGC6015, shows some oscillations in the rotation curve, mainly in the outer halo. Following fig. 7, those galaxies are clearly better fitted by extended isothermal-like halos compared to the contracted halos, given for lower W_0 values. The extended solutions provide a wide halo maximum followed by a flat rotation curve. This is suitable to fit the oscillations well on average, although the best-fit remains rather poor. The contracted solutions, in contrast, provide only a narrow maximum in the halo, followed by a Keplerian decreasing tail. The latter is clearly disfavored here. It is worth to note that the RAR model (and others such as NFW and DC14) are not appropriate to fit the oscillations, characterized through multiple maxima in the rotation curve.

In summary, we consider galaxies belonging to the first group as *appropriate* candidates because they allow to determine the W_0 value, although with some uncertainty. In contrast, galaxies belonging to the other two groups we consider as *inappropriate* candidates due to either a lack (e.g. DDO161) or an abundance (e.g. NGC6015) of information in the halo. This fact does not allow to determine the cutoff value, especially leaves the upper bound open. Though, in all cases it is possible to set a lower limit what clearly discards cuspy halos within the RAR model. Note that the lower limit in W_0 also sets a specific upper limit for the core mass.

3.4. *Milky Way*

We change now the focus to the Milky Way galaxy which is much better resolved than the SPARC galaxies. In particular, the widely covered radial extent, from the center to the outer halo, gives a better insight of the mass discrepancy.

The rotation curve for the Milky Way is given by Sofue (2013). In comparison to the SPARC data the baryonic components (bulge and disk) are given only analytically.

The bulge structure is composed of a main and an inner bulge. Each component is given by an exponential sphere model

$$\frac{\rho(r)}{\rho_b} = \mathrm{e}^{-r/R_b} \tag{27}$$

with a central density ρ_b and a length scale R_b. The mass is then given by $M(r) = \int_0^r 4\pi r^2 \rho(r) \mathrm{d}r$ and the circular velocity becomes

$$\frac{v^2(r)}{\sigma_b^2} = \frac{M(r)}{M_b}\frac{R_b}{R} \tag{28}$$

The scale factors are defined by $M_b = 4\pi\rho_b R_b^3$ and $\sigma_b^2 = GM_b/R_b$.

The disk is given by an exponential disk model where the surface density follows an exponential law,

$$\frac{\Sigma(r)}{\Sigma_d} = \mathrm{e}^{-r/R_d} \tag{29}$$

with the parameters Σ_d and R_d. The mass is then given by $M(r) = \int_0^r 2\pi r \Sigma(r) \mathrm{d}r$. Since the dynamics for an axial symmetric mass distribution differ from a spherical

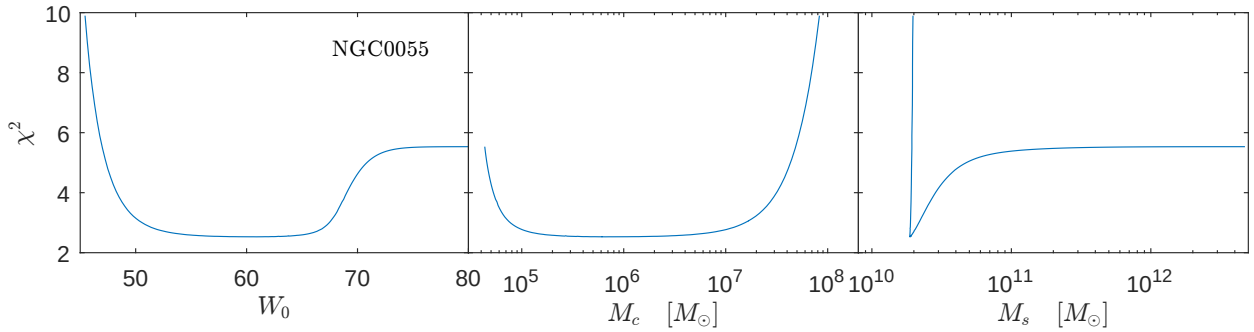

Figure 5. χ^2 profiles for NGC0055. There is a clear minimum for a total halo mass of $M_s \approx 2 \times 10^{10} M_\odot$. Due to the lack of information in the inner halo region the minimum corresponds to a valley in the core mass $10^5 \lesssim M_c \lesssim 10^7$, spanning a range of about 2 orders of magnitude. This uncertainty is also reflected in the cutoff parameter W_0. For relatively high values the solutions develop extended isothermal halo tails, which are clearly disfavored here. Solutions with relatively low W_0 values, corresponding here to highly cuspy profiles, are ruled out even stronger. Thus, in favor are solutions with mild surface effects.

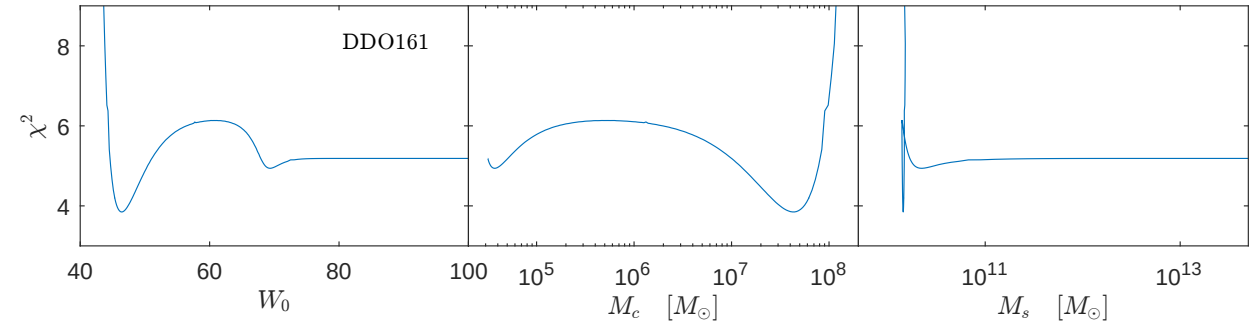

Figure 6. χ^2 profiles for DDO161. This galaxy is characterized through a rising rotation curve with a clear turning point. This *deficit* of information in the outer halo region makes is difficult to favor either extended (isothermal-like) or contracted halos. All solutions are suitable for fitting well the rotation curve with a rather small change in the χ^2 value. Solutions with lower W_0 values, corresponding to cuspy halos, are ruled out according to this analysis. With caution has to be taken the local minimum for relatively low W_0 values. This best-fit depends highly on the inner data points which are usually poorly constraint.

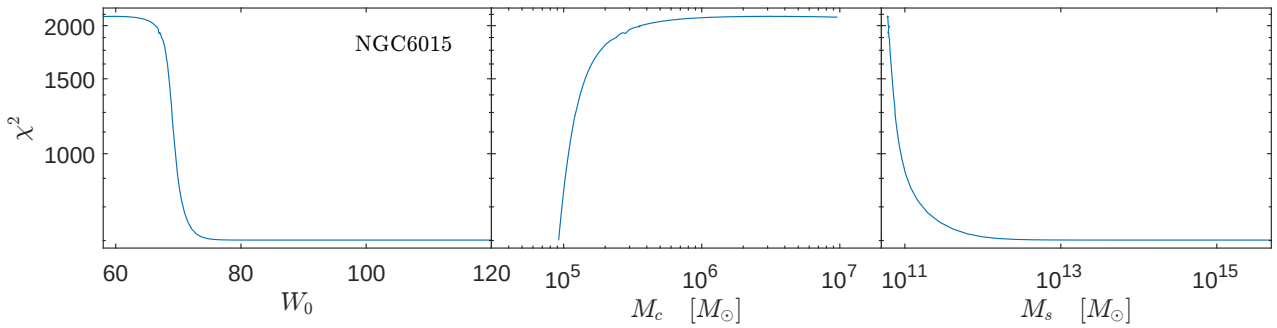

Figure 7. χ^2 profiles for NGC6015. This galaxy is characterized through an extended halo tail with oscillations. This *abundance* of information in the outer halo region clearly favors isothermal halos, corresponding to relatively high cutoff values. Those solutions provide extended halo tails with a wide halo maximum, suitable but insufficient for fitting well the rotation curve. Solutions with lower W_0 values are ruled out according to this analysis. The latter corresponds here to profiles with contracted halos without developing isothermal tails due to surface effects.

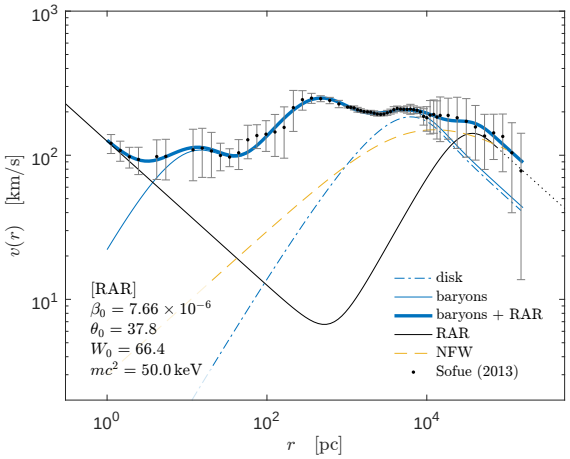

Figure 8. Rotation curves of the Milky Way galaxy. The observed velocities (black dots with error bars) are compared with the total velocity (thick solid line). The latter is composed of the baryonic component (dashed line), including a disk component (dot-dashed line), and the best-fit of the DM component, modeled with 50keV-RAR (thin solid line). For comparison, the NFW profile is added.

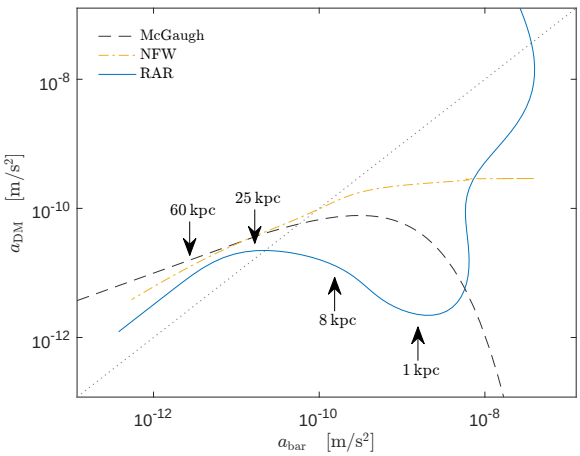

Figure 9. Radial acceleration correlation in the Milky Way galaxy. Results from the RAR model (solid line) are compared with McGaugh's empirical fit (dashed line) and NFW model (dot-dashed line). The dotted line describes where the centripetal acceleration of dark and baryonic matter are equal. Thus, in the top-left corner is the dark matter dominated region and in the bottom-right corner is the baryonic matter dominated region. The transition appears at about $2 \times 10^{-11}\,\mathrm{m/s^2}$. In the very high acceleration regime the RAR model predicts an increase of dark matter acceleration due to the degenerate dark matter core in the Galactic center.

component	total mass ($M_\odot$)	length scale (kpc)
inner bulge	5.5×10^7	4.07×10^{-3}
main bulge	9.7×10^9	0.137
disk	6.0×10^{10}	2.92

Table 1. Parameter for baryonic components of Milky Way. Note: baryonic and especially disk parameter imply RAR-DM component described by $mc^2 = 50\mathrm{keV}, \theta_0 \approx 37.8, W_0 \approx 66.4$ and $\beta_0 \approx 7.66 \times 10^{-6}$

symmetric mass distribution we have to use the circular velocity (on the equatorial plane) given by

$$\frac{v^2(r)}{\sigma_d^2} = 2y^2 \left[I_0(y)K_0(y) - I_1(y)K_1(y)\right] \qquad (30)$$

with the substitution $y = r/(2R_d)$ and the modified Bessel functions $I_n(x)$ and $K_n(x)$ (Binney & Tremaine 2008). The scale factors are defined by $M_d = 2\pi\Sigma_d R_d^2$ and $\sigma_d^2 = GM_d/R_d$.

In sum, the RAR model is able to describe the halo and explains simultaneously the compact object in the Galactic center, see fig. 8. Further details, especially concerning the supermassive black hole alternative in the Galactic center, are provided in Argüelles et al. (2018).

Here, we are mainly interested in the centripetal acceleration given by $a(r) = v^2(r)/r$. The length scales R_b and R_d as well as the masses M_b and M_d, describing the total bulge mass and disk mass, are provided in Sofue (2013) and table 1. Important attention has to be given to the disk parameters since they depend on the chosen dark matter model and have to be adjusted. Then, the baryonic contribution is the sum of inner bulge, main bulge and disk components. For the total contribution we have to add also the dark matter component.

In fig. 9 we find fundamental differences in the acceleration correlation compared to McGaugh's empirical fit. In the low acceleration regime (dark matter dominated) we obtain a linear proportionality what is due to the necessary strong cutoff in the halo. After that it follows the transition into the baryonic matter dominated regime with decreasing dark matter acceleration similar to McGaugh. However, in the high acceleration regime we have again an increase of dark matter acceleration because of the degenerate dark matter core, resembling a supermassive dark object, what is a fundamental feature of the RAR model.

For comparison, we have added the NFW model. The results show a similar trend in the low acceleration regime, but diverge towards a constant acceleration of the dark matter component in the high acceleration regime. Thus, all shown predictions (RAR, NFW and McGaugh) have a very different behavior in the baryonic dominated region.

3.5. *Correlations*

In this section we analyze different pairs of structural galaxy parameters obtained from the 50 keV-RAR model, such as θ_0 and β_0, the halo radius r_h and mass M_h as well as the core radius r_c and core mass M_c. Further, we are also interested in the total dark matter mass what needs a careful definition here.

Usually, mass distributions infinite in mass and space are truncated for example at a critical radius or density to obtain reasonable values. In that fashion, we define the *boundary mass* $M_b = M(r_b)$, being r_b the boundary radius where the density falls to the critical density of the Local Group ($10^{-5} M_\odot/\mathrm{pc}^3$).

On contrary, the RAR model provides naturally finite mass distributions via the cutoff parameter W_0. Thus, we define the *surface mass* $M_s = M(r_s)$, being r_s the natural surface radius where the density falls to zero. Important, for strong cutoff values we have total masses $M_s \approx M_b$.

It is important to emphasize that appropriate information about the halo, especially the outer halo, are needed to determine the cutoff parameter W_0. Thus, we divide the galaxy sample in two groups: galaxies with

- *appropriate* halo information ($M_{\mathrm{tot}} = M_b \approx M_s$)
- *inappropriate* halo information ($M_{\mathrm{tot}} = M_b \ll M_s$)

Here, *appropriate* refers to galaxies with sufficient information in the dark matter rotation curve (e.g. a clear maximum) while *inappropriate* refers either to a lack (e.g. no clear maximum) or to an abundance of information (e.g. oscillations in the outer halo).

Additionally, we introduce another group, the so called *flat-tail fits*. All candidates of this group have in common that their whole dark matter distribution is fitted well by the flat tail of the RAR model which implies no (or weak) evaporation. Due to the poor data of those galaxies we consider their results as an artifact of the fitting method. Thus, flat-tail fits produce dark matter distributions with too little halo radii and therefore too high halo and core masses. We speculate therefore that a proper choice of parameters, following the relation

$$\ln \frac{M_h}{M_\odot} \approx 2.02 \ln \frac{r_h}{\mathrm{pc}} + 5.10 \pm 1.54 \tag{31}$$

as found in the r_h-M_h plot (see left diagram of fig. 10), would produce adequate dark matter profiles, sufficient to describe the rotation curves with slightly different χ^2 values.

All considered solutions of the RAR model have always a degenerate core and a diluted halo. The core is defined as the first maxima in the rotation curve and the halo is defined as the second maxima. We obtain halo radii mainly in the interval $[10^3, 10^5]$pc and halo masses in the interval $[10^8, 10^{12}] M_\odot$. For the corresponding cores we obtain radii and masses in the intervals $[10^{-4}, 10^{-2}]$pc and $[10^3, 10^7] M_\odot$.

It is important to note that the quantum core is well described by a fully degenerate core. Analytically, we find the simple relation $M_c r_c^3 \sim m^{-8}$. Because we have set the particle mass, the mass-radius relation for the core has no predictive character here.

Of more interest is the core-halo relation for the mass. In that projection we clearly identify a distinction between the appropriate and the inappropriate halo groups. Both follow approx. the relation $M_h \sim M_c^2$ while the appropriate halo group shows a higher diversity. Following the best-fit analysis of NGC0055 (see. fig. 5), the diversity is most probably due to some uncertainty in the cutoff parameter W_0.

The group distinction with same characteristics is also visible in the θ_0-β_0 parameter space, see fig. 10. All best fits have a central degeneracy parameter in the degenerate regime, $\theta_0 \in [20, 50]$. For the central temperature parameter we obtain the range $[10^{-9}, 10^{-5}]$ which corresponds to the low temperature regime with negligible pressure effects.

Only for one galaxy (NGC4088) we find $\beta_0 \sim 10^4$ where pressure effects are not negligible any more. But that galaxy has a fundamental lack of information about the halo. Data shows only the inner part of the halo without any trend towards a maxima. This allows only to connect the galaxy with the r_h-M_h correlation group described by eq. (31). Without any information about the outer halo (e.g. maxima) it is impossible to predict a narrow window of halo radii and masses. In the following we consider this candidate as an outlier.

3.5.1. *Central core vs. total halo mass relation*

We move now to the $M_{\mathrm{BH}} - M_{\mathrm{tot}}$ relation (Ferrarese 2002; Kormendy & Bender 2011; Bogdán & Goulding 2015) where M_{tot} is the total dark matter halo mass and M_{BH} is the mass of the compact dark object at the center of galaxies. Traditionally, the central dark objects are assumed as SMBHs but here interpreted as dark matter quantum cores in the case of inactive galaxies. In the following we consider $M_{\mathrm{BH}} = M_c$, being $M_c = M(r_c)$ the quantum core mass. **?** showed that the RAR model is able to explain this relation for typical dwarf galaxies to normal ellipticals. Here, we extend the results

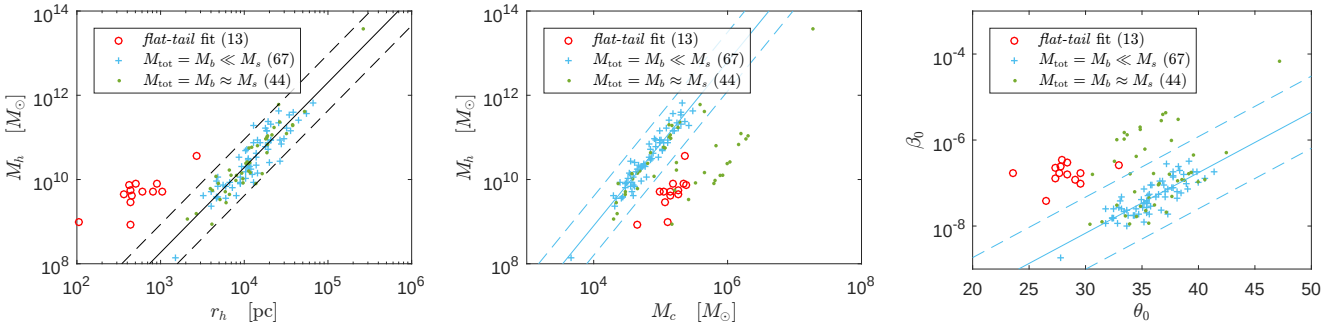

Figure 10. Parameter correlations for the best fits of the 50 keV-RAR model. The galaxy sample in every diagram is classified in three groups: (1) galaxies with appropriate halo information ($M_{\rm tot} = M_b \ll M_s$, dots), (2) with inappropriate halo information ($M_{\rm tot} = M_b \ll M_s$, crosses) and (3) with flat-tail fits which are considered as artifacts (open circles). (**left**) In the r_h-M_h plot we find a correlation with approx. $M_h \sim r_h^2$ (dots and crosses). In contrast to this correlation we may interpret the flat-tail fits as false fits. All of them have in common that the whole dark matter distribution was best-fitted with the flat tail of the RAR model, implying no (or weak) cutoff. Only for one galaxy (NGC4088) we find $\beta_0 \sim 10^4$ where pressure effects are not negligible any more. This *outlier* is due to the poor information about the halo where only the cored part without any maxima is available. (**middle**) Focusing on the M_c-M_h plot we clearly identify a distinction between the appropriate (dots) and the inappropriate halo group (crosses). Both follow approx. the relation $M_h \sim M_c^2$ while the appropriate halo group shows a higher diversity. (**left**) The distinction with the same characteristics is also visible in the θ_0-β_0 parameter space.

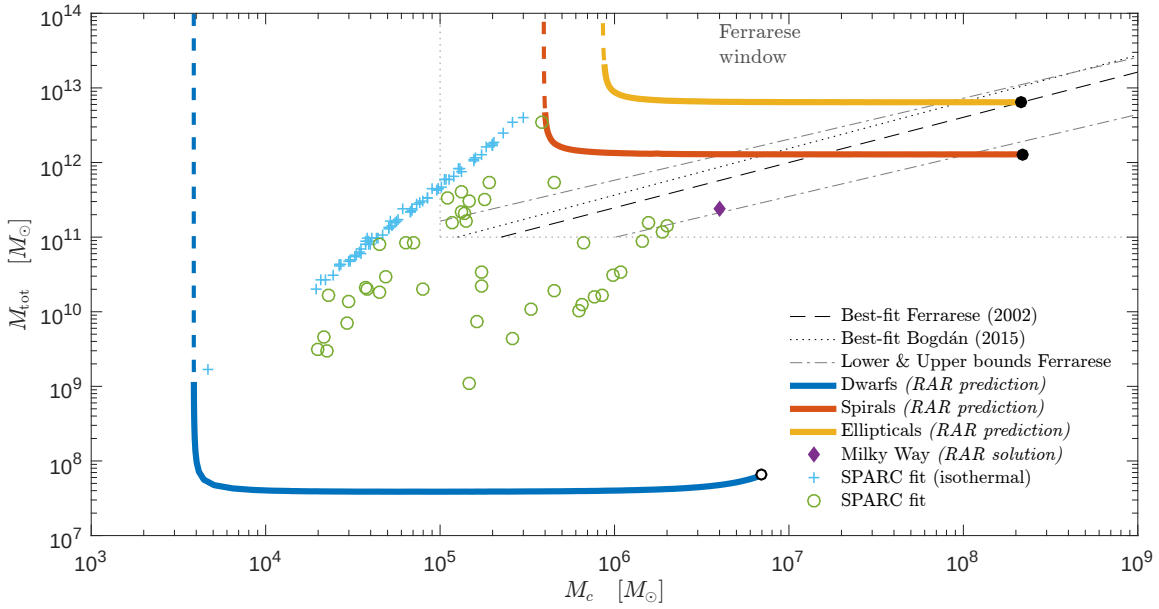

Figure 11. The different *predicted* color lines correspond for each galaxy type showing the ability of the three parametric (β_0, θ_0, W_0) RAR solutions for a particle mass $mc^2 \sim 50$ keV to be in agreement with the different $M_{\rm BH} - M_{\rm tot}$ relations considered in the literature (see **?** for details) and explicited in the picture box. The RAR predictions for typical spirals (red) and ellipticals (yellow) together with the Milky Way solution (diamond) lay within the *observable Ferrarese window*. The RAR prediction for typical dwarfs (blue) is located at the lower end of the M_c-$M_{\rm tot}$ plane, where data does not support. The black dots correspond to the critical core masses M_c^{cr} while the black circle indicates the limiting maximum core mass for dwarfs $M_c^{\rm max}$. The SPARC results of this paper are presented in two groups. Green circles correspond to galaxies with total masses $M_{\rm tot} = M_s < 10^{14} M_\odot$, being M_s the natural total mass of the obtained mass distribution. Light blue crosses correspond to total masses given by $M_{\rm tot} = M_b \ll M_s$, being M_b the mass at the boundary radius where the density falls to the critical density of the Local Group ($10^{-5} M_\odot/{\rm pc}^3$). Due to inappropriate halo information in the second group (light blue crosses) it is not possible to constrain the cutoff parameter W_0 what results in extended (isothermal) mass distributions with total masses $M_s \gg 10^{14} M_\odot$ which have to be truncated.

with predictions inferred from disk galaxies of the valid SPARC sample. The results are summarized in fig. 11.

Following the two definitions of enclosed mass (M_b and M_c, see above) we focus on the *appropriate* and *inappropriate* groups, excluding flat tail fits and outliers, to demonstrate the natural benefits of the RAR model. Especially the importance of the cutoff parameter W_0. The first group (green circles) corresponds to galaxies where the total mass is given by the surface mass, $M_{\rm tot} = M_s < 10^{14} M_\odot$. The second group (light blue crosses) corresponds to galaxies where the total masses given at the boundary radius, $M_{\rm tot} = M_b \ll M_s$.

The arbitrary upper mass limit $10^{14} M_\odot$ is applied to distinguish between realistic surface masses ($M_s < 10^{14} M_\odot$) and non-realistic ($M_s \geq 10^{14} M_\odot$). Clearly, spirals with masses above $10^{13} M_\odot$ are already highly improbable. And indeed, the prediction of the RAR model tells that SPARC spirals with appropriate halo information have natural total masses mainly below $10^{12} M_\odot$. Only one candidate has few $10^{12} M_\odot$.

Note that due to inappropriate information in the outer halo of the second group it is not possible to constrain the cutoff parameter W_0 what results in extended mass distributions with total masses $M_s \gg 10^{14} M_\odot$, see also fig. 7. Thus, it is necessary to truncate those extended mass distribution what results in a misleading narrow correlation in the $M_c - M_{\rm tot}$ relation. Instead, the RAR model predicts a much higher diversity rather than a narrow correlation according to the first group (green circles).

The majority of simulated galaxies has a total dark matter mass between $10^9 M_\odot$ and $10^{12} M_\odot$ while only a few are slightly more massive. The core mass spans a majority range between $10^4 M_\odot$ and few $10^6 M_\odot$. More important, the RAR model predicts here a break in the Ferrarese relation ($M_{\rm tot} \sim M_c^{0.6}$) at about $10^{11} M_\odot$, following $M_{\rm tot} \sim M_c^2$.

We want to emphasize that the second galaxy population (light blue crosses) has to be taken with caution since they don't provide appropriate information about the outer halo. We therefore recommend to rely mainly on the first galaxy population (green circles) with appropriate halo information.

3.5.2. *DM surface density relation*

Finally, we turn to the constant surface density (Donato et al. 2009)

$$\Sigma_{0D} = \rho_{0D} r_0 \approx 140^{+80}_{-50} M_\odot/{\rm pc}^2 \qquad (32)$$

This value is valid for about 14 orders of magnitude in absolute magnitude (M_B) where ρ_{0D} and r_0 are the *central* dark matter halo density at the one-halo-scale-length of the Burkert profile.

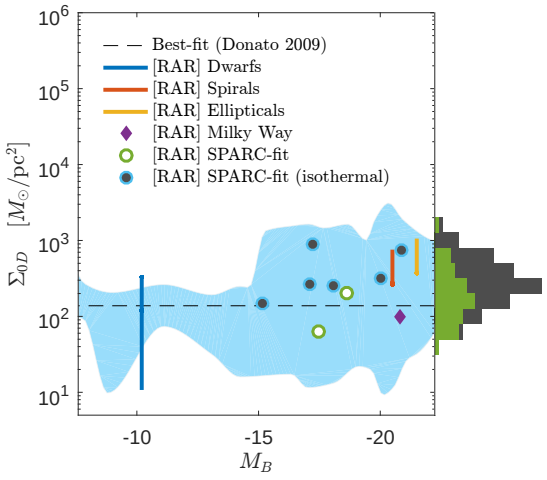

Figure 12. Prediction of the surface density for disk galaxies of valid SPARC samples. The absolute magnitude was taken from the Carnegie-Irvine Galaxy Survey, providing eight overlapping galaxies. The blue region indicates the delimited area by the 3σ error bars of all the data points used in Donato et al. (2009). The shown candidates include isothermal (blue outlined points) and non-isothermal (green circles) solutions, which are very well in agreement with the DM surface density observations. For comparison, the results are amended by RAR predictions for typical dwarfs, spirals and ellipticals (**?**). Although absolute magnitude information is incomplete, the predicted DM surface densities of the entire valid galaxy sample is within the range if the 3σ area as well. These full results are presented in a histogram (grey bars) with comparison to a subsample, including non-isothermal solutions (green bars). The majority of the latter sample is closer the the observationally inferred mean value of about $140 M_\odot$ pc^{-2}.

Note that the *center* in the Burkert model corresponds to the plateau in the RAR model, $\rho_{0D} \approx \rho_{\rm pl}$ where $\rho_{\rm pl}$ is defined at the first minima in the rotation curve. The relation between both one-halo scale lengths is $r_0 \approx 2/3\, r_h$. We thus calculate the product $2/3\, \rho_{\rm pl}\, r_h$ for each galaxy.

The absolute magnitude was taken from the Carnegie-Irvine Galaxy Survey, providing eight overlapping galaxies with the SPARC sample. These candidates are very well in agreement with the DM surface density observations, see fig. 12.

The central density results of the full galaxy sample (appropriate and inappropriate) is given as a histogram. Thus, the RAR model predicts for all valid candidates *central* surface densities within the 3σ uncertainty. It is worth to note that the spread is relatively high, although not in conflict with observables. This phenomena may be explained by the diversity, similar to the spread in the M_c-$M_{\rm tot}$ relation.

Considering only galaxies with appropriate halo information (green bars), we find that the majority is closer to the mean value of about $140 M_\odot$ pc^{-2}, compared to the full sample (dark gray bars).

4. SUMMARY AND CONCLUSION

We faced the intricate relation between the mass distribution of dark and baryonic matter for disk galaxies from a different perspective compared to the cosmological ΛCDM principles and MOND. Thus, we considered dark matter as a self-gravitating system composed of elementary fermions while the baryonic component was provided from the SPARC data base.

ACCELERATION CORRELATION

The radial acceleration correlation (McGaugh et al. 2016) as well as the equivalent mass discrepancy acceleration relation (McGaugh 2004, 2014) show clearly a link between the acceleration due to the baryonic matter and the acceleration due to dark matter. In the $a_{\rm bar}$-$a_{\rm DM}$ projection we found a linear relation between those two acceleration components rather than the proposed empirical fit based on the $a_{\rm bar}$-$a_{\rm tot}$ projection.

That RAR model is able to reproduce those acceleration correlations together with the their scatter. For comparison, we considered also two more DM models (NFW, DC14) which reproduce the empirical correlation qualitatively as well. In sum, we conclude that all considered DM models reproduce the correlation based on the average of many spiral galaxies of different Hubble type.

Nevertheless, focusing on individual galaxies we may extract more detailed information. Thus, we noticed fundamental deviations compared to the proposed radial acceleration correlation by McGaugh. Based on the representative NGC0055 it shows that many galaxies (of the SPARC database) don't follow strictly the given empirical formula. Despite an offset, NGC055 has a similar behavior to eq. (25) in the dark matter dominated region but deviates strongly in the transition into the baryonic matter dominated region with an abrupt decrease of the DM acceleration.

The deviations become more clear in the analysis of the much better resolved Milky Way. Here, we found a linear proportionality in the very low acceleration regime ($\lesssim 10^{-12}$m/s^2) in contrast to the empirical radial acceleration correlation. This deviation is due to the necessary strong cutoff.

Indeed, compared to the analysis of SPARC galaxies we know that spirals have very different halos regarding the cutoff. Those different cutoffs correspond to different slops of the radial acceleration correlation in the dark matter dominated regime. According to the RAR model we were able to identify several SPARC galaxies with a strong cutoff similar to Milky Way. But those galaxies (among many other) have a lack of information in the very outer halo (e.g. due to faint stars) what keeps the behavior in the very low acceleration regime ($\lesssim 10^{-12}$m/s^2) in secret.

Moving to the high acceleration regime, representing the baryonic matter dominated region, the prototype NGC0055 demonstrates clearly that the inner halo structure is important when the relevance of a cuspy or cored halo is considered. Thus, the new perspective of the radial acceleration correlation ($a_{\rm bar} - a_{\rm DM}$) is preferred compared to the original representation ($a_{\rm bar} - a_{\rm obs}$) which obscures the inner halo relation.

Finally, in the very high acceleration regime we predict an increase of the centripetal acceleration due to the quantum core in the galactic center, a fundamental feature of the RAR model. This is in clear contrast to the empirical correlation and the NFW model.

In sum, the unveiled deviations in the low and high acceleration regimes are a satisfying explanation for the large scatter in the radial acceleration correlation. The conclusion of the analysis is that the acceleration correlation of individual galaxies are more complicated than the empirical radial acceleration correlation suggest and that the RAR model is able to explain this phenomena based on fundamental physical principles.

GOODNESS OF FIT

The more profound understanding of the radial acceleration correlation is backed by a goodness of model analysis for 124 filtered galaxies of the SPARC data covering different Hubble types. We found that RAR and DC14 are similarly good while NFW is clearly disfavored here. This picture becomes even more clear when only magellanic galaxies are considered. On the contrary, non-megallanic galaxies are equally bad fitted with all models. This result implies a link between dark matter and the morphological type. Clearly, the type of the inner halo (cored or cuspy) may play an important role.

Spacial attention has to be given to galaxies with an oscillation in the rotation curve. All considered models (RAR as well as NFW and DC14) fail in fitting those rotation curves what appears mostly for non-magellanic types. This is not surprising, since all models have only one maxima bump by design. The oscillations of the RAR model with weak cutoff (or no cutoff in the limit) are too long ranged for a convenient explanation.

Comparing the RAR model with DC14 yields another interesting hint regarding baryonic-to-dark relations. We may consider DC14, a baryonic feedback motivated model, as an extension of the NFW model. Thus,

comparing DC14 and NFW implies that baryonic feedback mechanism is important in galaxy formation. But our RAR model fits the SPARC sample as good as DC14 although it doesn't consider any baryonic matter contribution nor any baryonic feedback mechanism. This leads to the speculation that baryonic feedback might be not so important for disk galaxies. The more probable scenario is that the RAR model enhanced with baryonic feedback mechanism would improve galaxy fitting significantly.

On the other hand, the RAR model is now confronted with the question why dark and baryonic matter distributions arrange in the way they obviously do. That relation seems to be encoded in the acceleration relation, its large scatter and, in particular, the *scatter shower* in the low acceleration regime of the dark matter component. The change of perspective from $a_{\rm bar}$-$a_{\rm obs}$ (original) to $a_{\rm bar}$-$a_{\rm DM}$ unveils the acceleration correlation on a wider spatial range and is therefore a good step forward. Since the RAR model considers only dark matter without any baryonic contribution nor feedback we are going to answer that fundamental question in a future work.

UNIVERSAL RELATIONS

Regarding dark-to-dark relations, we enriched the M_c-$M_{\rm tot}$ relation (**?**) with prediction for disk galaxies of the SPARC data base. The majority of the galaxies has a core mass between $10^4 M_\odot$ and few $10^6 M_\odot$ while the total masses span a range from $10^9 M_\odot$ to few $10^{12} M_\odot$. An important outcome of the results, compared to the $M_{\rm BH}$-$M_{\rm tot}$ relation (Ferrarese 2002), is a break in the relation at about $10^{11} M_\odot$, the bottom edge of the observable *Ferrarese window*. Of great interest would be therefore the extension of the relation down to dwarf galaxies what is under current investigation in our group.

We want to emphasize that the thinking of a narrow M_c-$M_{\rm tot}$ relation as suggested by Ferrarese (2002) might be misleading according the the predictability analysis of the RAR model, see also **?**. In particular, the model predicts a much higher diversity in the M_c-$M_{\rm tot}$ population what is supported by the SPARC results. On the other hand, the diversity is due to some uncertainty in the parameter space (e.g. the cutoff parameter W_0). To narrow those uncertainties better observations in the inner halo are needed.

The *constancy* of the surface density (Donato et al. 2009) for SPARC galaxies is also given within the RAR context. From the Carnegie-Irvine Galaxy Survey we have extracted the absolute magnitude for eight overlapping galaxies. The surface density predictions of that sub-sample are very well in agreement with observations. It is important to emphasize that the predicted surface density range, covering the full sample, remains within the 3σ uncertainty.

FUTURE PERSPECTIVE

We remind to interpret the results from isothermal galaxies, corresponding to $M_{\rm tot} = M_b \ll M_s$, with caution. Compared to the the remaining galaxies they have either a lack of information or short ranged oscillations in the outer halo what prohibits to constrain the cutoff parameter with certainty. The lack of information may be simply solved with future surveys while the oscillations, what may be regarded as an abundance of information, requires further investigations. A truncation (information filter) shortly after the first maxima in the rotation curve would certainly allow to compare with other galaxies, which provide only one maxima bump at best. We expect that such analysis will unveil more profound connections between the dark matter and the morphological type.

Although, the very different oscillations may be due to ongoing relaxation processes it might be worth to consider also multi-component halo models. It is probable that the RAR model enhanced with baryonic contributions will help in this analysis and thus to understand galactic structures.

Further, Kalinova et al. (2017) introduced recently a new dynamical classification of galaxies based on circular velocity curves. Such a classification based on the inferred dark matter rotation curves would be an interesting alternative to the classical morphological classification, which seems to be linked to dark matter profiles.

ACKNOWLEDGMENTS

A.K. is supported by the Erasmus Mundus Joint Doctorate Program by Grants Number 2014-0707 from the agency EACEA of the European Commission.

REFERENCES

Argüelles, C. R., Krut, A., Rueda, J. A., & Ruffini, R. 2018, Physics of the Dark Universe, 21, 82, doi: 10.1016/j.dark.2018.07.002

Argüelles, C. R., & Ruffini, R. 2014, International Journal of Modern Physics D, 23, 1442020, doi: 10.1142/S0218271814420206

Argüelles, C. R., Ruffini, R., & Fraga, B. M. O. 2014a, Journal of Korean Physical Society, 65, 809, doi: 10.3938/jkps.65.809

Argüelles, C. R., Ruffini, R., Siutsou, I., & Fraga, B. 2014b, Journal of Korean Physical Society, 65, 801, doi: 10.3938/jkps.65.801

Binney, J., & Tremaine, S. 2008, Galactic Dynamics, 2nd edn. (Princeton University Press), 920

Bogdán, Á., & Goulding, A. D. 2015, ApJ, 800, 124, doi: 10.1088/0004-637X/800/2/124

Cappellari, M., Emsellem, E., Krajnović, D., et al. 2011, MNRAS, 413, 813, doi: 10.1111/j.1365-2966.2010.18174.x

Chae, K.-H., Bernardi, M., & Sheth, R. K. 2017, ArXiv e-prints. https://arxiv.org/abs/1707.08280

Chavanis, P.-H. 2004, Physica A Statistical Mechanics and its Applications, 332, 89, doi: 10.1016/j.physa.2003.09.061

Cintio, A. D., Brook, C. B., Dutton, A. A., et al. 2014, Monthly Notices of the Royal Astronomical Society, 441, 2986, doi: 10.1093/mnras/stu729

de Blok, W. J. G., Walter, F., Brinks, E., et al. 2008, AJ, 136, 2648, doi: 10.1088/0004-6256/136/6/2648

Di Cintio, A., & Lelli, F. 2016, MNRAS, 456, L127, doi: 10.1093/mnrasl/slv185

Donato, F., Gentile, G., Salucci, P., et al. 2009, MNRAS, 397, 1169, doi: 10.1111/j.1365-2966.2009.15004.x

Ferrarese, L. 2002, ApJ, 578, 90, doi: 10.1086/342308

Ferrarese, L., & Merritt, D. 2000, ApJL, 539, L9, doi: 10.1086/312838

Hernquist, L. 1990, ApJ, 356, 359, doi: 10.1086/168845

Ingrosso, G., Merafina, M., Ruffini, R., & Strafella, F. 1992, A&A, 258, 223

Kalinova, V., Colombo, D., Rosolowsky, E., et al. 2017, MNRAS, 469, 2539, doi: 10.1093/mnras/stx901

Katz, H., Lelli, F., McGaugh, S. S., et al. 2016, ArXiv e-prints. https://arxiv.org/abs/1605.05971

Keller, B. W., & Wadsley, J. W. 2016, ArXiv e-prints. https://arxiv.org/abs/1610.06183

King, I. R. 1966, AJ, 71, 64, doi: 10.1086/109857

Klein, O. 1949, Reviews of Modern Physics, 21, 531, doi: 10.1103/RevModPhys.21.531

Kormendy, J., & Bender, R. 2011, Nature, 469, 377, doi: 10.1038/nature09695

Kroupa, P. 2015, Canadian Journal of Physics, 93, 169, doi: 10.1139/cjp-2014-0179

Lelli, F., McGaugh, S. S., & Schombert, J. M. 2016, AJ, 152, 157, doi: 10.3847/0004-6256/152/6/157

—. 2017a, ArXiv e-prints. https://arxiv.org/abs/1702.04355

Lelli, F., McGaugh, S. S., Schombert, J. M., & Pawlowski, M. S. 2017b, ApJ, 836, 152, doi: 10.3847/1538-4357/836/2/152

Ludlow, A. D., Benitez-Llambay, A., Schaller, M., et al. 2016, ArXiv e-prints. https://arxiv.org/abs/1610.07663

McGaugh, S. 2014, Galaxies, 2, 601, doi: 10.3390/galaxies2040601

McGaugh, S., Lelli, F., & Schombert, J. 2016, ArXiv e-prints. https://arxiv.org/abs/1609.05917

McGaugh, S. S. 2004, ApJ, 609, 652, doi: 10.1086/421338

McGaugh, S. S., Schombert, J. M., Bothun, G. D., & de Blok, W. J. G. 2000, ApJL, 533, L99, doi: 10.1086/312628

Merafina, M., & Ruffini, R. 1989, A&A, 221, 4

Navarro, J. F., Benítez-Llambay, A., Fattahi, A., et al. 2016, ArXiv e-prints. https://arxiv.org/abs/1612.06329

Navarro, J. F., Frenk, C. S., & White, S. D. M. 1996, ApJ, 462, 563, doi: 10.1086/177173

Rubin, V. C., Ford, W. K. J., & . Thonnard, N. 1980, ApJ, 238, 471, doi: 10.1086/158003

Ruffini, R., Argüelles, C. R., & Rueda, J. A. 2015, MNRAS, 451, 622, doi: 10.1093/mnras/stv1016

Salucci, P. 2016, ArXiv e-prints. https://arxiv.org/abs/1612.08857

Santos-Santos, I. M., Brook, C. B., Stinson, G., et al. 2016, MNRAS, 455, 476, doi: 10.1093/mnras/stv2335

Shapiro, S., & Teukolsky, S. 2008, Black Holes, White Dwarfs and Neutron Stars: The Physics of Compact Objects (Wiley). https://books.google.it/books?id=CB2kZ-vMhaoC

Siutsou, I., Argüelles, C. R., & Ruffini, R. 2015, Astronomy Reports, 59, 656, doi: 10.1134/S1063772915070124

Sofue, Y. 2013, PASJ, 65, 118, doi: 10.1093/pasj/65.6.118

Tenneti, A., Mao, Y.-Y., Croft, R. A. C., et al. 2017, ArXiv e-prints. https://arxiv.org/abs/1703.05287

Tolman, R. C., & Ehrenfest, P. 1930, Physical Review, 36, 1791, doi: 10.1103/PhysRev.36.1791

Tully, R. B., & Fisher, J. R. 1977, A&A, 54, 661